Am J Transl Res 2020;12(6):2463-2472
www.ajtr.org /ISSN:1943-8141/AJTR0104866

Original Article

Carrying epirubicin on nanoemulsion containing algae and cinnamon oils augments its apoptotic and anti-invasion effects on human colon cancer cells

Mayson H Alkhatib[1], Majidah A Aljadani[1,2], Sawsan H Mahassni[1]

[1]Department of Biochemistry, Faculty of Science, King Abdulaziz University, PO Box 42801, Jeddah 21551, Saudi Arabia; [2]Department of Chemistry, Science and Arts College, Rabigh Campus, King Abdulaziz University, PO Box 42801, Jeddah 21551, Saudi Arabia

Received November 13, 2019; Accepted April 20, 2020; Epub June 15, 2020; Published June 30, 2020

Abstract: The nanotherapeutics holds great potential in cancer therapy since they may consist of more than one anticancer agent that has a different mechanism of action. The present study aimed to incorporate the epirubicin (EPI) into a nanoemulsion containing the algae and cinnamon oils (ALG-CN-EPI) using ultrasonication technique. The apoptotic efficacy of ALG-CN-EPI was assessed in the HCT116 human colon cancer cells using the assays of CCK-8, DNA fragmentation, reactive oxygen species (ROS) generation, and Annexin V-FITC/PI while the anti-invasion effect of ALG-CN-EPI was determined by the transwell invasion assay. The zeta average diameters and zeta potential of the nano-suspensions of ALG-CN-EPI, measured by the zetasizer, were 117.2 ± 3.02 nm and -1.810 ± 0.07 mV, respectively. Results of the apoptotic evaluation revealed that the half-maximal inhibitory concentration (IC_{50}) of ALG-CN-EPI (0.7 ± 0.21 μM) was distinctly lower than that of free EPI (6.00 ± 1.56 μM). The DNA fragmentation of HCT116 cells was amplified by a factor of 8 ± 0.24 when treated with ALG-CN-EPI but it did not considerably differ when treated with the free EPI (1.13 ± 0.31). Additionally, cells treated with ALG-CN-EPI resulted in a significant elevation of the intracellular ROS production and higher percentages of late apoptotic cells relative to the EPI treated cells. ALG-CN-EPI treatment suppressed the invasion ability of HCT116 cells to (32.98 ± 3.28)%, whereas the invasion ability of EPI exposed cells was only reduced to about (56 ± 1.81)%. In conclusion, the resulted new nanotherapeutics (ALG-CN-EPI) has potentiated the antitumor activity of EPI.

Keywords: Nanotherapeutics, chemotherapeutic agent, antitumor activity, DNA fragmentation, zetasizer, essential oils

Introduction

After lung and breast cancer; colon cancer becomes the third most prevalent cancer in the world and the second leading cause of death worldwide [1]. The anthracycline, epirubicin (EPI), is a 4'-epimer of doxorubicin which is one of the most widely used chemotherapeutic agents that affect several cancers like breast, ovarian, gastric, bladder and colon cancers [2]. The cytotoxicity of EPI stems from its ability to intercalate the DNA strands and thereby suppress the synthesis of DNA and RNA [3]. However, cardiotoxicity, allergic reactions, and non-specific distributions in normal tissues limit its clinical applications [4].

In the last decades, the targeted drug delivery system has attracted much attention in cancer treatment. Nanosystems like liposomes, micelles, nanoemulsions, nanoparticles, dendrimers, and nanocapsules were investigated to deliver the drugs to the target site. EPI was delivered in different nanocarrier systems. It was encapsulated in oligosaccharide capped gold nanoparticle (AuNPs) [5], polymeric micelles [6], poly-lactide-co-glycolic acid (PLGA) nanoparticles [7], Surface-modified-HCl liposomes [8] and adsorbed nanodiamonds [9].

Among the different nanocarrier systems, nanoemulsions (NEs) have the potential to deliver the drug to the tumor site. Nanoemulsions, which are heterogeneous dispersion systems that are composed of oil, water, surfactants and/or co-surfactants, have emerged as one of the promising approaches to enhance the delivery of the cytotoxic agents. They are gaining

popularity because of their ease of formation, the small particle size of the oil droplets generally < 100 nm which targeted release of the drugs or therapeutic molecules at the site of action, high stability, and high bioavailability [10].

Essential oils (ESSOs) were found to possess anticancer potential by acting on various pathways and cellular mechanisms [11]. Furthermore, delivering ESSOs with the conventional drugs in NE formula had enhanced the efficacy of the therapeutic applications and thus reduce its adverse side effects [12]. The present study was performed to evaluate the actual potential of EPI encapsulated in algae (ALG) and cinnamon (CN) NE delivery system on the HCT116 cancer cells.

Materials and methods

Chemicals

Tween 80 and span 20 were purchased from Al-rowad Modern Establishment for the Supply of Medical Equipment (Jeddah, KSA). Cinnamon oil was purchased from the Secret of Egypt (Sharm El Sheikh, Egypt). Algae oil was obtained from iHerb (@iherb). Epirubicin (EPI) was procured from Ebewe Pharmaceuticals Ltd (Unterach. Austria). Penicillin Streptomycin, dimethyl sulfoxide (DMSO), Fetal Bovine serum, Trypsin-EDTA 0.25%, and Dulbecco's Modification of Eagles Medium (DMEM) were purchased from UFC biotechnology, Inc. (Jeddah, KSA).

Assay kits

Cell counting kit-8 (CCK-8) (Lot. No LE612) was purchased from Dojindo Molecular Technologies (Japan). Annexin V-FITC/PI Apoptosis Detection Kit (Cat. No MBS668896) was purchased from MyBioSource (California, USA). Cell Death Detection Elisa Plus (Lot. No 1931-5700) was purchased from Roche (Mannheim, Germany). QCMTM 24-Well Collagen-Based Cell Invasion Assay (Cat. No. ECM 551) was purchased from Merck KGaA (Darmstadt, Germany). 2,7-Dichlorodihydrofluorescein diacetate (DCFH-DA) (Cat. No. 85155) was purchased from Cayman (ANN ARBOR, USA).

Preparation of the nanoemulsion formulations

The nanoemulsion (ALG-CN) was produced by mixing the weight percentages of 2% ALG oil, 2% CN oil, 7% Tween 80, 3% Span 20 and 86% of phosphate buffer (pH 8) followed by ultrasonication using ultrasonicator (OMNI International, SONIC Ruptor 4000, Georgia, USA) with an amplitude of 40% between 15 and 30 min. During sonication, the temperature of the ALG-CN formula was maintained at 25°C by cooling in an ice bath. It should be noted that all of the tested concentrations of EPI-loaded ALG-CN were prepared by dissolving the desired amount of EPI in the ALG-CN formula.

Particle characterization

The particle size, polydispersity index (PDI), and zeta potential of the formulated ALG-CN and 1 mg/mL of ALG-CN-EPI were evaluated by the dynamic light scattering (DLS) at 25°C using a Malvern Zetasizer (Malvern Instruments Ltd., Malvern, UK).

Turbidity measurements

The effect of temperature on the turbidity of ALG-CN, expressed in a nephelometric (NTU) scale, was detected using a turbidity meter with a tungsten-filament lamp light source (Sper Scientific, Taiwan). The turbidities of ALG-CN were determined at different temperatures in the range of (5-85)°C for the heating and cooling cycle. The temperatures were scanned at a rate of 1°C/min.

In vitro drug release study

The *in vitro* drug-release profiles of free EPI and AL-CN-EPI were evaluated by the dialysis method. 2 mL of the desired sample was sealed in a dialysis bag and incubated in 250 mL phosphate buffer (pH 7) and stirred at 100 rpm and 37°C. 2 mL of sample solution was collected at different time intervals (1, 2, 3, 4, 5, 6, 7, 8 h). At each predetermined time, 2 mL of the sample was taken and replaced with 2 mL fresh phosphate buffer. The absorbance of the collected samples was measured by the UV-visible spectrophotometer (Thermo Fisher Scientific, US).

Cell culture

The HCT116 cell line, procured from America Type Tissue Culture Collection (Manassas, VA, USA), was cultured in a 25 cm^2 cell culture flask containing DMEM supplemented with 10% (v/v) FBS and 1% (v/v) penicillin-streptomycin followed by incubation in a 5% CO_2/95% humidi-

fied atmosphere at 37°C. Cells were dissociated using 0.25% trypsin and re-suspended in fresh media once every 2 days.

Cell growth inhibition assay

Cell inhibition assay was implemented using cell counting kit-8, CCK-8. Cells were grown in a full supplemented DMEM growth medium containing 10% FBS and 1% antibiotic mixture. 1×10^4 cells were seeded in a 96 well plate at which each well contained 100 µL of culture media. Then, cells were incubated in a 5% CO_2/95 % humidified atmosphere at 37°C for 24 h. After that, the old media was removed and replaced with fresh growth media containing seven different concentrations of EPI (0.1-10 µM) and four different concentrations of ALG-CN and ALG-CN-EPI (0.1-1.5 µM). Following 24 h incubation, 5 µL of CCK-8 reagent was added for each well, mixed gently and left for 3 h in the incubator. The absorbance (A) was recorded at 450 nm using a microplate reader (BioTek, US). Wells containing culture media and untreated cells were respectively considered as blank and control. The percentages of cell inhibitory rate were determined by the following equation: Inhibitory rate (%) = $100 - ((A_{\text{Treated cells}} - A_{\text{Blank}})/(A_{\text{control}} - A_{\text{Blank}}) \times 100)$.

Cell morphology visualization

Light microscopy was utilized to observe the alterations in the morphology of the cells subjected to different treatments. Cells, at a density of 1×10^4, were seeded in a 96-well plate at which each well contained 100 µL of culture media. Cells were treated with 100 µL of different concentrations of the desired drug formula for 24 h. After that, cells were washed twice with 100 µL of PBS and fixed by the addition of 100 µL of 4% formaldehyde for 10 min. Then, cells were stained with 100 µL of 5% Coomassie blue for 10 min. Finally, cells were washed with tap water twice after discarding the stain and left to dry at room temperature, 25°C. The cellular morphology was observed under light microscopy and images were captured using an Olympus microscope (Olympus Corporation, Tokyo, Japan).

Detection of DNA fragmentation in apoptotic cells

The extent of DNA fragmentation was measured using the Cell Death Detection ELISA kit Plus. In each well, 1×10^4 Cells were seeded in a flat-bottomed 96-well plate containing 100 µL of growth media and were placed in a CO_2 incubator for 24 h at 37°C. Then, cells were treated with 100 µL of the IC_{50} for EPI, ALG-CN, and ALG-CN-EPI. After 24 h incubation, cells were washed with cold PBS, collected and lysed for 30 min using lysis buffer, provided by the kit manufacturer. The lysate was centrifuged at 200 × g for 10 min. The supernatant (20 µL) was added into a streptavidin-coated microplate well. After that, 80 µL of the immunoreagent solution, consisted of anti-histone-biotin and anti-DNA-peroxidase, prepared prior to use in the ratio of 1:1 v/v, was added into each well and incubated with gentle shaking for 2 h. Wells were washed three times for 20 min with ABTS substrate solution, provided by the kit's manufacturer. The DNA fragmentation expressed as the enrichment of histone-associated mono- and oligo-nucleosomes released into the cytoplasm, was determined at 405 nm against the substrate solution as a blank. The enrichment factor was calculated by the following equation: Enrichment factor = $(A_{\text{Treated Cells}} - A_{\text{Blank}})/A_{\text{control}}$.

Detection of apoptosis using Annexin V-FITC/PI assay

Cells (2×10^5) were seeded in a 6-well plate and incubated for 24 h at 37°C and 5% CO_2. Then, cells were treated with 1000 µL of EPI, ALG-CN, and ALG-CN-EPI (IC_{50} value) for 24 h. After that, cells were harvested and washed twice with 1 × PBS and re-suspended in 100 µL of 1 × binding buffer at a concentration of 1×10^6 cells/mL. After transferring the solution from each set into the flow cytometry-tubes, 5 µL of Annexin V FITC and 5 µL of PI were added. In each tube, the mixture was mixed gently and incubated in the dark for 20 min at room temperature followed by the addition of 400 µL of the binding buffer. Finally, cells were visualized by fluorescence microscopy (Leica CRT6000, Germany) and analyzed by BD FACSAria™ III Flow Cytometer (BD Biosciences, US).

Measurement of reactive oxygen species (ROS)

2', 7'-Dichlorofluorescin diacetate (DCFH-DA) was used to measure the ROS generation. DCFH-DA is a cell-permeable non-fluorescent probe which deacetylated by cellular esterases

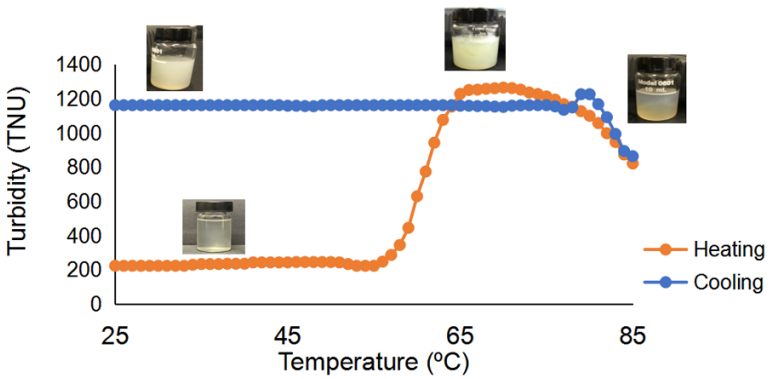

Figure 1. Influence of heating-cooling rate on the turbidity of ALG-CN expressed in a nephelometric (NTU) scale and detected using a turbidity meter.

to a non-fluorescent compound, which oxidized by ROS into 2', 7'-dichlorofluorescein (DCF). Cells (1×10^4) were seeded in a flat-bottomed 96-well plate containing 100 µL of growth media and were placed in a CO_2 incubator for 24 h at 37°C. Then, cells were treated with 100 µL of the IC_{50} for EPI, ALG-CN, and ALG-CN-EPI. After 24 h incubation, cells were washed with PBS. After that, 5 µL of DCFH-DA was added to each well and incubated for 30 min. Fluorescence was monitored at an excitation wavelength of 485 nm and an emission wavelength of 528 nm using a fluorescence microplate reader (BioTek, US).

Transwell invasion assay

Cells (2×10^5) were seeded in a 6-well plate and incubated for 24 h at 37°C and 5% CO_2. After that, cells were treated with 1000 µL of EPI, ALG-CN, and ALG-CN-EPI (IC_{50} value) for 24 h. Then, cells were washed twice with PBS and collected using centrifugation at 1400 rpm for 10 min. The pellets were re-suspended in serum-free media and transferred into the upper chambers of 24-well plate containing 8-mm pore size chamber inserts. The lower chambers were filled with 500 µL serum-free medium. After 24 hours of incubation at 37°C, the non-invading cells were removed with cotton swabs. Invasive cells at the bottom of the membrane were stained with 5% Coomassie blue and photographed using a light microscope. After that, the stained cells were extracted with 10% acetic acid and transferred to a 96-well microtiter plate. The absorbance was measured at 560 nm using a microplate reader (BioTek, US).

Statistical analysis

Data were expressed as the mean ± SD. Statistical analysis was performed using MegaStat (version 10.3, Butler University, Indianapolis, IN). Differences in means were evaluated by one-factor analysis of variance (ANOVA) test and Tuckey's post-hoc analysis to identify the *P*-values for the pairwise *t*-test. The independent samples *t*-test was used to compare two independent groups. The differences between the samples were considered when the *P*-value was less than 0.05.

Results

Turbidity determination

With the aim to determine the stability of the produced ALG-CN, the influence of the heating-cooling cycle on the variation in turbidity was implemented as exhibited in **Figure 1**. During heating, the turbidity remained relatively low and constant until 55°C. However, the turbidity increased steeply by further increasing the temperature from 55°C to 72°C followed by a gradual decrease in the turbidity when the temperatures were raised above 72°C. Upon cooling, the system remained highly turbid and separated into a white cream layer and watery serum layer when it was kept at room temperature.

Zetasizer measurements of ALG-CN and ALG-CN-EPI

According to the zetasizer measurements shown in **Table 1**, the z-average diameter of ALG-CN-EPI was markedly greater than ALG-CN ($P < 0.001$). The zeta potentials for both of ALG-CN and ALG-CN-EPI were negatively charged. However, the magnitude of the zeta potential of ALG-CN-EPI was more than that of ALG-CN ($P < 0.01$). Interestingly, the polydispersity indexes (PDI) for the nanodroplets of ALG-CN and ALG-CN-EPI, which indicate the discrepancies among the droplet sizes, were insignificant.

Table 1. Zetasizer measurements of ALG-CN and ALG-CN-EPI

Formulation	Zeta average diameter (nm)	PDI	Zeta potential
ALG-CN	44.89 ± 1.11	0.024 ± 0.010	-0.218 ± 0.52
ALG-CN-EPI	117.2 ± 3.02	0.026 ± 0.012	-1.810 ± 0.07

The significant differences between the formulas, assessed by measuring the *P*-values using the independent *t*-test, were classified to $^{**}P < 0.001$ and $^{***}P < 0.0001$.

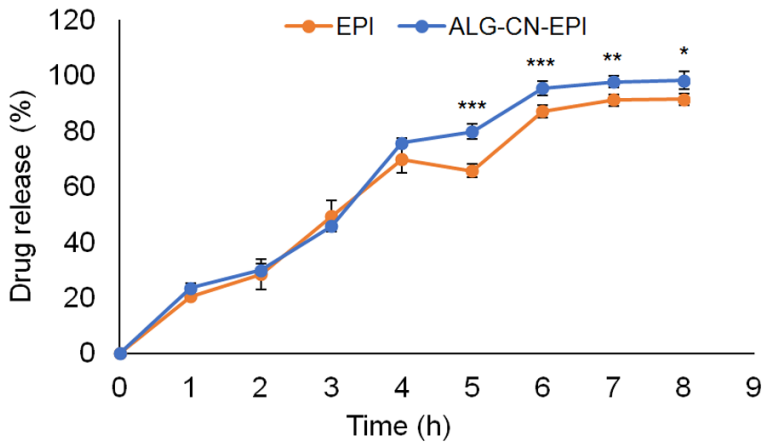

Figure 2. The drug release profile of the EPI and ALG-CN-EPI in phosphate-buffered saline (50 mM, pH 7). *Error bars* represent the ± standard deviation. The significant differences between EPI and ALG-CN-EPI at each time, assessed by measuring the *P*-values using the independent *t*-test, were classified to $^{*}P < 0.01$, $^{**}P < 0.001$ and $^{***}P < 0.0001$.

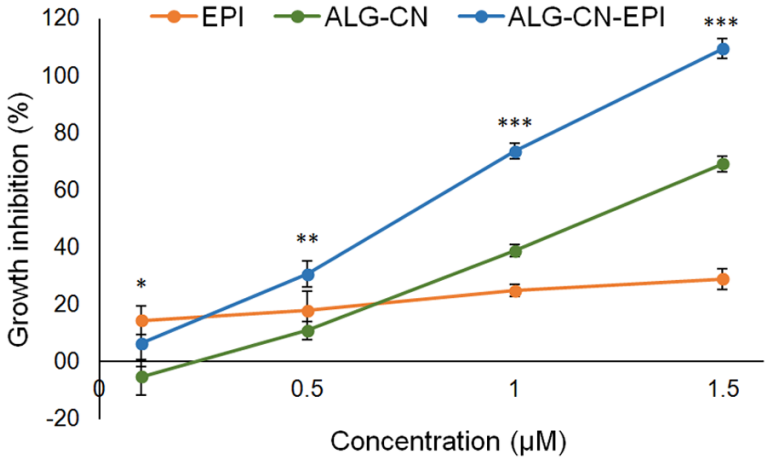

Figure 3. Cell growth inhibition rates in HCT116 treated with different concentrations of EPI, ALG-CN, and ELG-CN-EPI followed by incubation in a CO_2 incubator at 37°C for 24 h. The cell growth inhibitory rate was measured using the CCK-8 assay. *Error bars* represent the ± standard deviation. The significant differences among the three tested formulas at each concentration, assessed by measuring the *P*-values using one-factor ANOVA and Tuckey's post-hoc analysis to identify the *P*-values for the pairwise *t*-test, were classified to $^{*}P < 0.01$, $^{**}P < 0.001$ and $^{***}P < 0.0001$.

In vitro release of EPI and ALG-CN-EPI

The cumulative release percentage profiles of EPI and ALG-CN-EPI are shown in **Figure 2**. It should be notified that the *in vitro* release profile of ALG-CN was similar to the profile of ALG-CN-EPI (data not shown). The shape of the curves for both EPI and ALG-CN-EPI indicates a sustained release. After 5 h, the release of ALG-CN-EPI was markedly higher than that of EPI. In particular, the cumulative release percentages of ALG-CN-EPI and EPI within 8 h were ~98 and 91%, respectively.

Cell growth inhibition assay

In order to assess the inhibitory effect of different concentrations for EPI, ALG-CN, and ALG-CN-EPI on the proliferation of HCT116 cancer cells, CCK-8 assay was performed as shown in **Figure 3**. Apparently, the percentages of growth inhibition were directly proportional to the subjected concentration of both of ALG-CN, and ALG-CN-EPI. However, there were no considerable differences in the growth inhibition of HCT116 when subjected to different concentrations of EPI. Among the tested formulas, the best inhibition effect was observed when ALG-CN-EPI was applied at concentrations above 0.50 μM. The minimal inhibitory concentrations (IC_{50}) of ALG-CN and ALG-CN-EPI were 1.27 and 0.7 μM, respectively which were much less than that of EPI (6.00 μM).

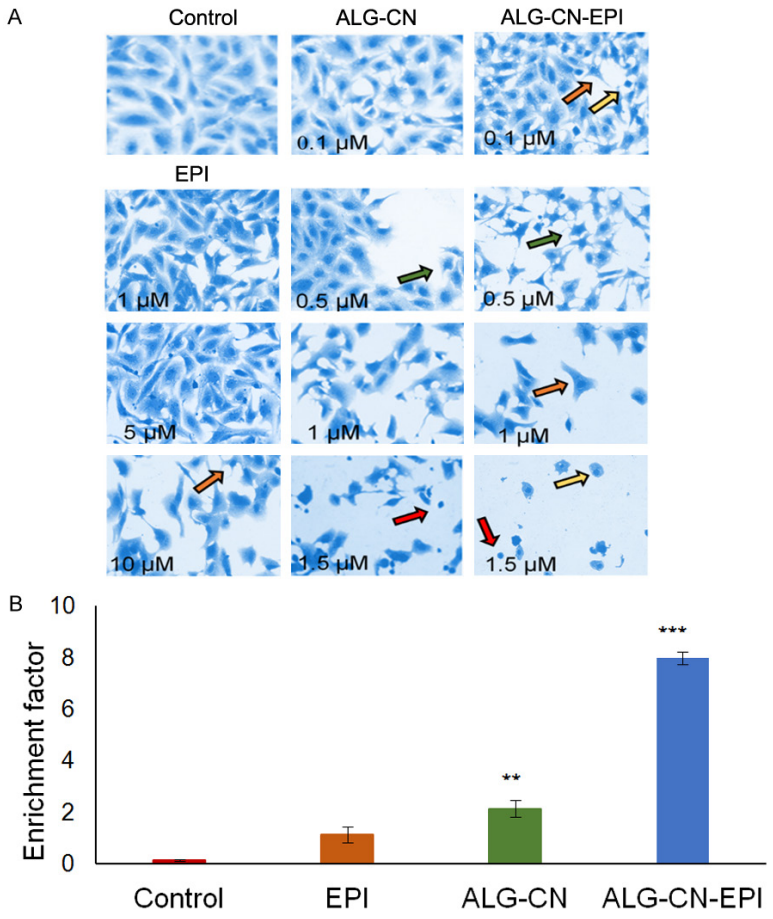

Figure 4. A. Morphological changes of HCT116 cells treated with different concentrations of tested formulas followed by incubation in a CO_2 incubator at 37°C for 24 h and viewed under an inverted light microscope (40 × magnifications). Arrows colored with orange, green, yellow and red display membrane blebbing, cell shrinkage, condensed nuclei, and apoptotic bodies, respectively. B. The percentage of apoptotic cells estimated by measuring the level of DNA fragmentation using the cell death detection ELISA ^{Plus} assay. Apoptosis is reflected by the enrichment of nucleosomes in the cytoplasm shown on the y-axis. *Error bars* represent the ± standard deviation. The significant differences between the control and each tested formula, assessed by measuring the *P*-values using the independent *t*-test, were classified to $^{**}P < 0.001$ and $^{***}P < 0.0001$.

Assessment of apoptosis by cell morphology and DNA fragmentation

The morphological observations of the affected HCT116 cells after treated with different concentrations of EPI, ALG-CN, and ALG-CN-EPI for 24 h were exhibited in **Figure 4A**. All treated cells had endured similar common features for apoptosis such as membrane blebbing, cell shrinkage, DNA fragmentation, and chromatin condensation. In contrast, the untreated cells (control) maintained most of their morphological features as a normal shape with an intact and large vesicular nucleus. Under these conditions, however, we also found a significant enhancement of oligonucleosomal DNA fragmentation, a finding that is generally accepted as a hallmark of apoptosis.

The quantification of the number of apoptotic cells was identified by measuring the enrichment factor of the nucleosomes in the cancer cells as elaborated in **Figure 4B**. ALG-CN-EPI treatment had markedly increased the DNA fragmentation in HCT116 cells ($P < 0.001$), which reached up to 8-fold when compared to the control. There was also a significant enhancement ($P < 0.01$) observed in the enrichment factor of the ALG-CN treated cells relative to the control group. In contrast, cells treated with EPI did not considerably endure significant fragmentation of DNA relative to the control.

Detection of apoptosis using Annexin V-FITC/PI assay

Annexin V-FITC/PI double-staining technique was used to further identify the stages of apoptosis induced by the tested formulas when subjected to the HCT116 cells as shown in **Figure 5A**, **5B**. What can be clearly seen in **Figure 5C** is the high percentage of late apoptotic cells in the ALG-CN-EPI treated cells when compared to the other tested formulas. In contrast, EPI treated cells consisted of higher percentages of early apoptotic and necrotic cells relative to the other NE formulas. Among the tested formulas, ALG-CN treated cells contained the highest percentages of viable cells which were markedly diminished when HCT116 cells were subjected to ALG-CN-EPI treatment.

Assessment of the intracellular ROS generation

The generation of ROS, caused by the tested formulas, was assessed by a fluorescent probe

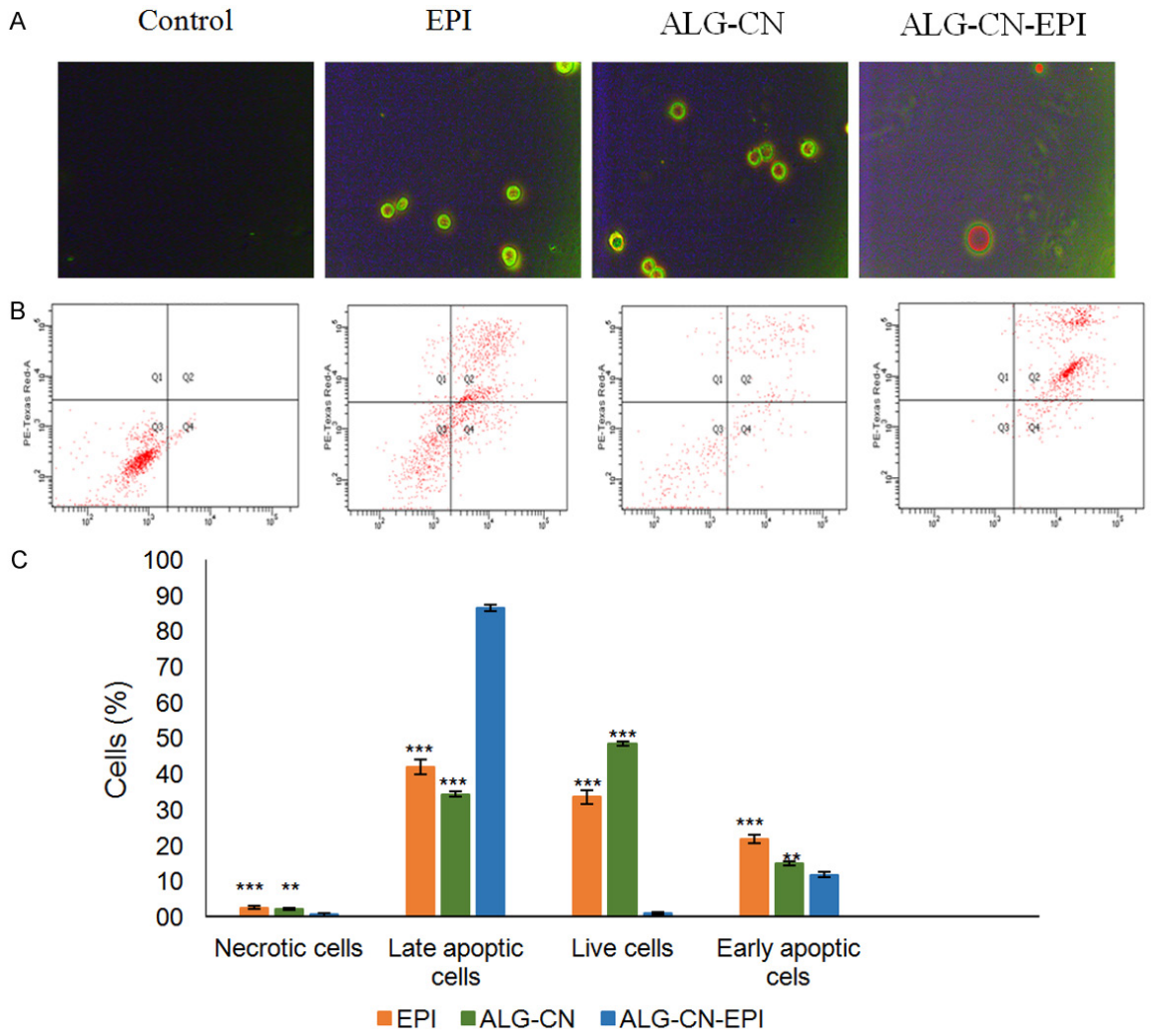

Figure 5. Annexin V-FITC/PI assay for the apoptosis induction in HCT116 cells when untreated (control) and treated with the IC_{50} of EPI, ALG-CN, and ALG-CN-EPI followed by incubation in a CO_2 incubator at 37°C for 24 h. A. Fluorescent microscopy images of the tested cells (magnification 20 ×). B. Dot plots representing the distribution of the cells enduring different stages of apoptosis: viable (Q3), early apoptotic (Q4), late apoptotic (Q2) and necrotic (Q1). C. Bar diagrams for the calculated percentages of the cells using FACSDiva software version 8.0. *Error bars* represent the ± standard deviation. The significant differences between ALG-CN-EPI and the other tested formula, assessed by measuring the *P*-values using the independent *t*-test, were classified to $^{**}P < 0.001$ and $^{***}P < 0.0001$.

DCFH-DA that detected the intracellular ROS (**Figure 6**). Cells treated with ALG-CN and ALG-CN-EPI resulted in a significant elevation of the intracellular ROS production relative to the EPI treated cells.

Transwell invasion assay

Invasion assay was performed to detect the invasive ability of HCT116 cells (**Figure 7**). Apparently, the invasive ability of the HCT116 cells was significantly suppressed (32.98 ± 3.28)% when cultured with the IC_{50} of ALG-CN-EPI. In contrast, HCT116 exposed to EPI resulted in about (56 ± 1.81)% decrease in the number of invasive cells.

Discussion

Although the essential oils are effective natural anticancer agents and have many beneficial properties such as anti-inflammatory, antimicrobial...etc., their clinical applications are still limited due to their poor bioavailability caused by their hydrophobicity that restrains their permeation into the targeted tissues [13]. Nanoemulsions provide effective methods in maximizing the solubility of the hydrophobic

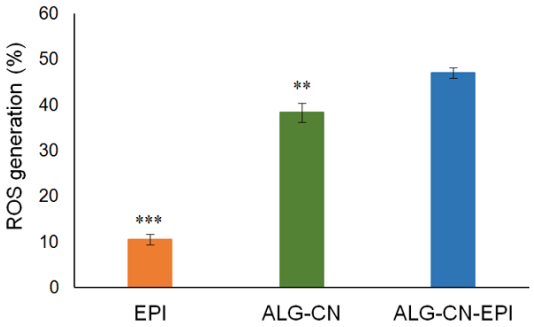

Figure 6. Percentages increase of the ROS generated from the HCT 116 cells when treated with the IC_{50} of the tested formulas followed by incubation in a CO_2 incubator at 37°C for 24 h, stained with DCFH-DA fluorescent dye and detected by a fluorescence microplate reader. *Error bars* represent the ± standard deviation. The significant differences between ALG-CN-EPI and the other tested formula, assessed by measuring the *P*-values using the independent *t*-test, were classified to $^{**}P < 0.001$ and $^{***}P < 0.0001$.

drugs in aqueous solutions containing few amounts of surfactants/cosurfactant. Additionally, the combination of the essential oils with chemotherapeutic agents in nanoemulsions might improve their therapeutic potentials through synergistic effects [14].

In this study, the resulted ALG-CN nanoemulsion was formulated using ultrasonication, which is an efficient technique for formulating stable nanoemulsions with very small droplet size and low PDI [15]. According to the turbidity study, ALG-CN was less stable above 55°C and appeared creamy which might be caused by the dehydration of the head groups of non-ionic surfactants that result in the extensive droplet coalescence. As a consequence, large droplets that scattered light strongly might get formed [16].

According to the antiproliferation assay, the IC_{50} of EPI (6.00 ± 1.56) μM was less than the IC_{50} of ALG-CN-EPI (0.70 ± 0.21) μM by 8.60 folds. The potential activity of the ALG-CN-EPI can be attributed to the small size of the formula which helps in the enhancement of the cellular permeation and improves the accumulation in the target site [17]. Additionally, the rapid drug release of ALG-CN-EPI may play a role in the drug selectivity to the cancer cells. Furthermore, the inclusion of ALG and CN oils in the nanoemulsion formula may potentiate the anti-cancer activity of EPI. Actually, The ALG and CN oils have an anticancer activity with different mechanisms. Yang *et al.* [18] had recently demonstrated that the cytotoxicity activity of a nanoemulsion, consisting of deionized water, Tween 80, Span 80, coffee and ALG oils, was attributed to its ability to arrest the cell cycle at G2/M and inhibit the growth of melanoma cell. A recent study had reported that the antineoplastic activity of CN oil against head and neck squamous cell carcinoma stem from the suppression of the epidermal growth factor receptor tyrosine kinase [19].

The induction of apoptosis in HCT116 cells treated with EPI, ALG-CN, and ALG-CN-EPI was monitored by the analysis of the morphological changes in the cells using light microscopy, DNA fragmentations assay, and annexin V-FITC/PI staining using flow cytometry. It had been found that ALG-CN-EPI had a greater apoptotic effect than EPI, which implies that the cellular accumulation of the nano-colloidal droplets of ALG-CN-EPI was augmented relative to the EPI. Similar to our findings, combining the ifosfamide with the lemon and salvia oils in a nanoemulsion had developed its antitumor activity against HeLa and MCF-7 cells [14]. Moreover, mixing mitomycin C with chamomile oil based on nanoemulsion had considerably improved its cytotoxicity on the HeLa cells and eliminated its hematotoxicity in mice inoculated with tumor [12, 20].

Furthermore, our study showed that ALG-CN and ALG-CN-EPI promoted ROS production in HCT116 cells. It has been demonstrated previously that the presence of various essential oils had caused ROS induction [21]. Accumulating reports revealed a direct association between ROS production and DNA damage leading to apoptosis [22-24]. The invasion study was employed in order to assess the metastatic ability of the treated cancer cells. The invading cells might be impeded by blocking the channels of the K^+ ions that play a major role in promoting the invasion process [25]. In the present study, the invasion ability of HCT116 cells treated with ALG-CN-EPI was significantly decreased indicating that the drug formula affected the K^+ ions channels. Furthermore, nanoparticles (NPs), evaluated as carriers of conventional drug therapies, were designed to treat cancer metastasis. According to the study of Murphy *et al.* [26], loading doxorubicin in the

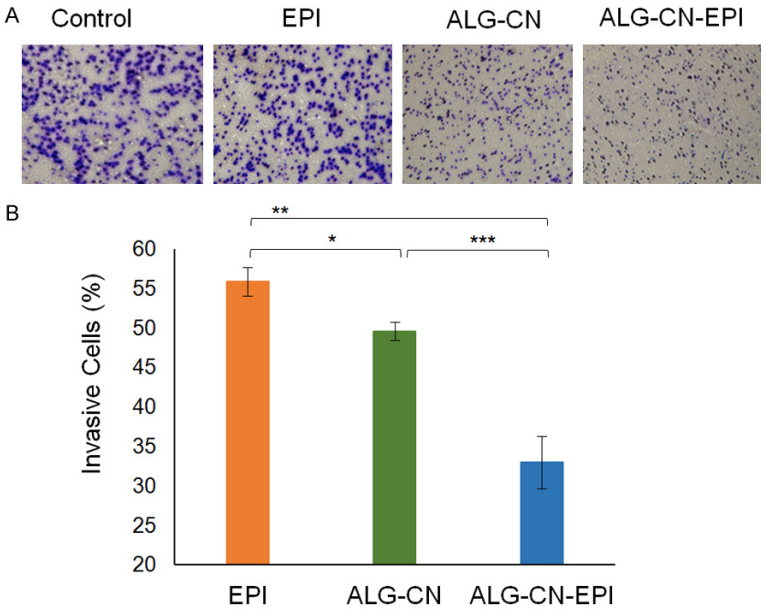

Figure 7. Invasion of HCT116 cells, determined by the transwell assay, in response to treatments with the IC_{50} for EPI, ALG-CN, and ALG-CN-EPI formulas followed by incubation in a CO_2 incubator at 37°C for 24 h. A. Light microscopy images of the invaded cells stained with Coomassie blue (20 × magnifications). B. Percentages of the invaded cells exposed to the tested formulas. *Error bars* represent the ± standard deviation. The significant differences between each two tested formulas, assessed by measuring the *P*-values using the independent *t*-test, were classified to $*P < 0.01$, $**P < 0.001$ and $***P < 0.0001$.

polymeric NPs had resulted in a 15-fold increase in the antimetastatic activity when compared to the free drug.

Conclusions

The results collectively revealed that the mixing of EPI with ALG-CN has considerably improved its anticancer efficacy and eliminated the invasion ability of HCT116 cells. It is recommended to perform more experimental studies in animal models in order to elaborate on the adverse side effects of the new formulation.

Acknowledgements

This project was funded by the Deanship of Scientific Research (DSR), King Abdulaziz University, Jeddah, under grant No. (DF-607-247-1441). The authors, therefore, acknowledge DSR technical and financial support.

Disclosure of conflict of interest

None.

Address correspondence to: Mayson H Alkhatib, Department of Biochemistry, Faculty of Science, King Abdulaziz University, Jeddah, Saudi Arabia. Tel: +966-599240526; E-mail: mhalkhatib@kau.edu.sa

References

[1] Bray F, Ferlay J, Soerjomataram I, Siegel RL, Torre LA and Jemal A. Global cancer statistics 2018: GLOBOCAN estimates of incidence and mortality worldwide for 36 cancers in 185 countries. CA Cancer J Clin 2018; 68: 394-424.

[2] Taghdisi SM, Danesh NM, Ramezani M, Lavaee P, Jalalian SH, Robati RY and Abnous K. Double targeting and aptamer-assisted controlled release delivery of epirubicin to cancer cells by aptamers-based dendrimer in vitro and in vivo. Eur J Pharm Biopharm 2016; 102: 152-158.

[3] Tariq M, Alam MA, Singh AT, Iqbal Z, Panda AK and Talegaonkar S. Biodegradable polymeric nanoparticles for oral delivery of epirubicin: in vitro, ex vivo, and in vivo investigations. Colloids Surf B Biointerfaces 2015; 128: 448-456.

[4] Devi PR, Kumar CS, Selvamani P, Subramanian N and Ruckmani K. Synthesis and characterization of Arabic gum capped gold nanoparticles for tumor-targeted drug delivery. Mater Lett 2015; 139: 241-244.

[5] Chen X, Han W, Zhao X, Tang W and Wang F. Epirubicin-loaded marine carrageenan oligosaccharide capped gold nanoparticle system for pH-triggered anticancer drug release. Sci Rep 2019; 9: 6754-6763.

[6] Takemae K, Okamoto J, Horise Y, Masamune K and Muragaki Y. Function of epirubicin-conjugated polymeric micelles in sonodynamic therapy. Front Pharmacol 2019; 10: 546-555.

[7] Tariq M, Alam MA, Singh AT, Panda AK and Talegaonkar S. Improved oral efficacy of epirubicin through polymeric nanoparticles: pharmacodynamic and toxicological investigations. Drug Deliv 2016; 23: 2990-2997.

[8] Liu L, Mu LM, Yan Y, Wu JS, Hu YJ, Bu YZ, Zhang JY, Liu R, Li XQ and Lu WL. The use of functional epirubicin liposomes to induce pro-

grammed death in refractory breast cancer. Int J Nanomedicine 2017; 12: 4163-4167.
[9] Wang X, Low XC, Hou W, Abdullah LN, Toh TB, Mohd Abdul Rashid M, Ho D and Chow EK. Epirubicin-adsorbed nanodiamonds kill chemoresistant hepatic cancer stem cells. ACS Nano 2014; 8: 12151-12166.
[10] Shaker DS, Ishak RA, Ghoneim A and Elhuoni MA. Nanoemulsion: a review on mechanisms for the transdermal delivery of hydrophobic and hydrophilic drugs. Sci Pharm 2019; 87: 17-50.
[11] Blowman K, Magalhães M, Lemos M, Cabral C and Pires I. Anticancer properties of essential oils and other natural product. Evid Based Complement Alternat Med 2018; 2018: 1-12.
[12] Al-Otaibi W, Alkhatib M and Wali A. Evaluation of antitumor activity and hepatoprotective effect of mitomycin C solubilized in chamomile oil nanoemulsion. Anticancer Agents Med Chem 2019; 19: 1232-1242.
[13] Nair A, Amalraj A, Jacob J, Kunnumakkara AB and Gopi S. Non-curcuminoids from turmeric and their potential in cancer therapy and anticancer drug delivery formulations. Biomolecules 2019; 9: 13-48.
[14] Alkhatib M, AlMotwaa S and Alkreathy H. Incorporation of ifosfamide into various essential oils-based nanoemulsions ameliorates its apoptotic effect in the cancers cells. Sci Rep 2019; 9: 695-703.
[15] Ghosh V, Mukherjee A and Chandrasekaran N. Ultrasonic emulsification of food-grade nanoemulsion formulation and evaluation of its bactericidal activity. Ultrason Sonochem 2013; 20: 338-344.
[16] Saberi AH, Fang Y and McClements DJ. Formation of thermally reversible optically transparent emulsion-based delivery systems using spontaneous emulsification. Soft Matter 2015; 11: 9321-9329.
[17] Tummala S, Kumar MS and Pindiprolu SK. Improved anti-tumor activity of oxaliplatin by encapsulating in anti-DR5 targeted gold nanoparticles. Drug Deliv 2016; 23: 3505-3519.
[18] Yang CC, Hung CF and Chen BH. Preparation of coffee oil-algae oil-based nanoemulsions and the study of their inhibition effect on UVA-induced skin damage in mice and melanoma cell growth. Int J Nanomedicine 2017; 12: 6559-6580.
[19] Yang XQ, Zheng H, Ye Q, Li RY and Chen Y. Essential oil of Cinnamon exerts anti-cancer activity against head and neck squamous cell carcinoma via attenuating epidermal growth factor receptor-tyrosine kinase. J BUON 2015; 20: 1518-1525.
[20] Alkhatib M, Al-Otaibi W and Wali A. Antineoplastic activity of mitomycin C formulated in nanoemulsions-based essential oils on HeLa cervical cancer cells. Chem Biol Interact 2018; 291: 72-80.
[21] Yu GJ, Choi IW, Kim GY, Hwang HJ, Kim BW, Kim CM, Yoo Y and Choi YH. Induction of reactive oxygen species-mediated apoptosis by purified Schisandrae semen essential oil in human leukemia U937 cells through activation of the caspase cascades and nuclear relocation of mitochondrial apoptogenic factors. Nutr Res 2015; 35: 910-920.
[22] Hildeman DA, Mitchell T, Kappler J and Marrack P. T cell apoptosis and reactive oxygen species. J Clin Invest 2003; 111: 575-581.
[23] Su J, Lai H, Chen J, Li L, Wong YS, Chen T and Li X. Natural borneol, a monoterpenoid compound, potentiates selenocystine-induced apoptosis in human hepatocellular carcinoma cells by enhancement of cellular uptake and activation of ROS-mediated DNA damage. PLoS One 2013; 8: e63502.
[24] Bhardwaj M, Kim NH, Paul S, Jakhar R, Han J and Kang SC. 5-Hydroxy-7-methoxyflavone triggers mitochondrial-associated cell death via reactive oxygen species signaling in human colon carcinoma cells. PLoS One 2016; 11: e0154525.
[25] Veiseh O, Kievit FM, Ellenbogen RG and Zhang M. Cancer cell invasion: treatment and monitoring opportunities in nanomedicine. Adv Drug Deliv Rev 2011; 63: 582-596.
[26] Murphy EA, Majeti BK, Barnes LA, Makale M, Weis SM, Lutu-Fuga K, Wrasidlo W and Cheresh D. Nanoparticle-mediated drug delivery to tumor vasculature suppresses metastasis. Proc Natl Acad Sci U S A 2008; 105: 9343-9348.